Int. J. Heat Mass Transfer. Vol. 36, No. 1, pp. 201–212, 1993
Printed in Great Britain

0017-9310/93 $5.00 + 0.00

A study of circumferentially-heated and block-heated heat pipes—I. Experimental analysis and generalized analytical prediction of capillary limits

JOSEPH SCHMALHOFER and AMIR FAGHRI
Department of Mechanical and Materials Engineering, Wright State University, Dayton, OH 45435, U.S.A.

(*Received* 12 *August* 1991 *and in final form* 25 *November* 1991)

Abstract—An experimental analysis of several operating parameters for a low temperature, copper–water heat pipe under uniform circumferential heating and block heating has been performed. The transient wall and vapor temperature behavior under different step heat inputs was determined. The experimental and analytical capillary limit and the rise time to a 60°C vapor temperature was found for both modes of heating.

1. INTRODUCTION

ELECTRONIC circuitry has traditionally been cooled by forced or natural convection, but as VLSI techniques have improved, the amount of excess heat generated by electronic chips has increased dramatically. It has been proposed to employ heat pipes to remove this heat by directly attaching the heat pipe to the surface of the chip. This heating situation will be termed 'block heating', as opposed to 'circumferential heating', which is normally associated with cylindrical heat pipes.

Experimental data have been reported for circumferential heating in both low- and high-temperature heat pipe applications under steady-state and transient operation. The most recent efforts in this respect were those of Faghri and Thomas [1] concerning annular heat pipes and Faghri and Buchko [2] for heat pipes with multiple heat sources. The experimental heat pipe used by Rosenfeld [3] consisted of a cylindrical pipe with a narrow block-heated evaporator called a line heater, and a circumferentially symmetric condenser section with a sintered-metal artery wick. The liquid-filled artery was on the side opposite the line heater. The experimental data taken from this heat pipe were strictly for steady-state operation, and no data were reported concerning the transient operating characteristics or capillary limit.

In the present study, the wall and centerline vapor temperatures and heat output were obtained for a circumferentially-heated and block-heated heat pipe. The objectives were to determine the elapsed time to reach a 60°C vapor temperature from an initial ambient temperature of 21°C after a step heat input, observe any differences in the steady-state wall and vapor temperatures, and compare the experimental capillary limit of the heat pipe over a range of vapor temperatures to the generalized analytical capillary limits developed in this study for block-heated pipes.

2. EXPERIMENTAL SET-UP AND TEST PROCEDURES

The schematic of the experimental heat pipe test stand is shown in Fig. 1. The low temperature heat pipe consisted of a copper pipe sealed with copper end caps containing two wraps of copper screen of 1968.5 meshes per meter for the wick and degassed, distilled water as the working fluid. The heat pipe was 1000 mm long with a 25.4 mm outer diameter and a 1.7 mm wall thickness. Table 1 shows the physical dimensions and properties of the materials used in the experimental low temperature copper–water heat pipe.

Two Minco Thermofoil heaters, each with a maximum heat input of 250 W at 250°C, were used as evaporator heat sources. The circumferential heater covered the entire circumference of the pipe from 0.015 to 0.079 m measured from the evaporator end cap, and the block heater covered the top half of the circumference from 0.089 to 0.216 m as shown in Fig. 2. The surface area of the circumferential heater was $5.107 \times 10^{-3}\,m^2$ and the block heater $5.080 \times 10^{-3}\,m^2$. This resulted in the heat fluxes from the heaters being within 0.5% for a fixed total heat input. The heat input was determined by measuring the voltage and the amperage with a FLUKE-77 digital multimeter. The combined uncertainty of the power reading was $\pm 3\%$. The voltage was regulated using a variable AC transformer. A vapor temperature of 60°C was chosen as the reference temperature to keep the heaters from exceeding their safe operating temperatures.

A Neslab CFT-25 chiller supplied water at a constant inlet temperature to the condenser. The chiller had a maximum capacity of 500 W over a coolant temperature range of 5–30°C. A calibrated flowmeter was used to determine the volumetric flow rate of water through the condenser. The heat pipe was mounted on an optical bench to facilitate leveling.

NOMENCLATURE

A	cross-sectional area [m^2]
C	ratio of the screen mesh diameter to the opening width of the screen, d/w_s
D	ratio of the screen mesh wire diameter to the wick thickness, d/t_w
D_v	dynamic pressure coefficient [$N\ m^{-2}\ W^{-2}$]
d	screen mesh wire diameter [m]
d_i	container inner diameter [m]
d_w	wick inner diameter [m]
F	frictional pressure coefficient [$N\ m^{-2}\ W^{-1}\ m^{-1}$]
$(f_v Re_v)$	drag constant
g	gravity constant [$m\ s^{-2}$]
h_{fg}	latent heat [$J\ kg^{-1}$]
K	wick permeability [m^2]
L	length of heat pipe [m]
L_a	total adiabatic section length [m]
L_c	condenser length [m]
L_e	evaporator length [m]
L_{eff}	effective total transport length [m]
P	pressure [$N\ m^{-2}$]
P_c	capillary pressure [$N\ m^{-2}$]
P_{cm}	maximum capillary pressure [$N\ m^{-2}$]
P_n	normal hydrostatic pressure [$N\ m^{-2}$]
Q	axial heat transport [W]
$Q_{c,max}$	analytical capillary limit [W]
Q^*	local axial heat flux rate [W]
Q'	axial heat rate per unit circumferential length [$W\ m^{-1}$]
R_{ave}	average liquid-wick radius [m]
$r_{h,v}$	hydraulic radius of vapor flow [m]
r_p	wick pore radius [m]
t_w	wick thickness [m]
w_s	screen mesh opening width [m]
z	axial location [m].

Greek symbols

ε	wick porosity
θ	circumferential angle [rad]
μ	dynamic viscosity [$kg\ m^{-1}\ s^{-1}$]
ρ	density [$kg\ m^{-3}$]
σ	surface tension [$N\ m^{-1}$]
ψ	heat pipe inclination angle [rad].

Subscripts

l	liquid
ref	reference
v	vapor
w	wick.

The condenser, coolant plumbing, and heat pipe were insulated with at least two inches of Fiberfrax ceramic fiber insulation.

The heat pipe was instrumented with 14 outer wall and 6 vapor centerline Type K and Type T thermocouples, which had uncertainties of $\pm 0.5^{\circ}C$. Two Type K thermocouples measured the inlet and outlet temperatures of the condenser coolant. Figure 3 shows the physical locations of the thermocouples.

The elapsed time required for the copper–water heat pipe to reach a vapor temperature of 60°C after the application of a uniform step heat input of 25, 50, 75, 100, 125, and 150 W was determined for circumferentially-heated and block-heated operations. After the vapor temperature exceeded 65°C, the coolant flow was started through the condenser and the heat pipe was allowed to reach a steady-state condition. The inlet temperature of the coolant was

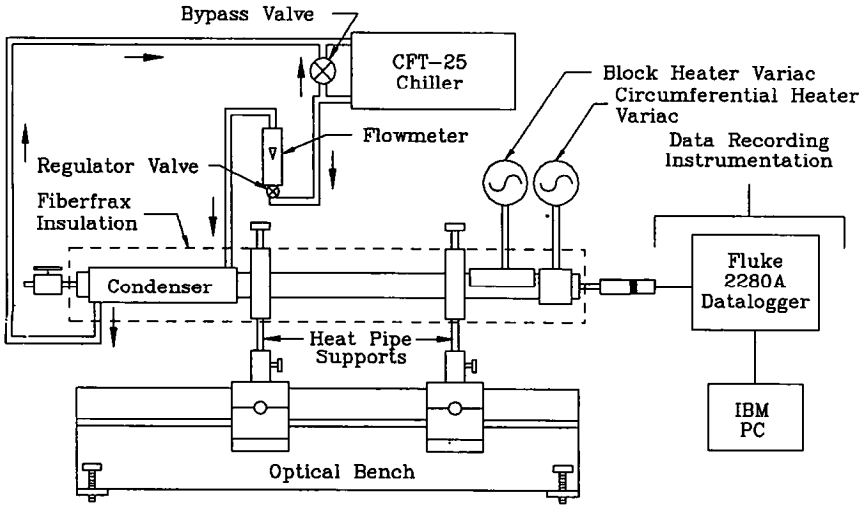

FIG. 1. Schematic of experimental setup.

Table 1. Physical dimensions and material properties of the circumferentially-heated and block-heated heat pipe

Pipe and end cap material	Copper
Pipe O.D.	2.54×10^{-2} m
Pipe I.D.	2.20×10^{-2} m
Pipe length	1.0 m
End cap thickness	3.175×10^{-3} m
Wick material	Copper
Screen mesh number	1.97×10^{3} m^{-1}
Wick thickness	7.12×10^{-4} m
Wick pore radius	1.78×10^{-4} m
Vapor core diameter	2.058×10^{-2} m
Working fluid	Distilled water
Fluid charge	40 cm^3
Circumferential evaporator length	6.4×10^{-2} m
Block evaporator length	1.27×10^{-1} m
Circumferential mode transport length	6.01×10^{-1} m
Block mode transport length	4.61×10^{-1} m
Condenser length	2.69×10^{-1} m

held constant at 27.5 ± 2.5°C, and the flow rate was adjusted to maintain vapor temperatures of 65–75°C. Higher heat inputs were not tested because the peak wall temperature under the heaters would have exceeded their design limitations. Wall and vapor temperatures and the heat output from the condenser were recorded. Between tests, a minimum of 8 h was allowed for the heat pipe to cool to room temperature.

The capillary limit was defined as the heat input at which the wall temperature directly underneath the heater exhibited a continuous sudden temperature rise. This condition occurs when the amount of condensate being evaporated exceeds that being brought into the evaporator region by the capillary action of the wick, which dries out the wick and causes the evaporator wall temperature to increase.

For both heating modes, the capillary limit was determined by starting the heat pipe with a heat input of 50 W until the desired vapor temperature was reached. The coolant was then regulated through the condenser to keep the vapor temperature constant. For the tests performed at vapor temperatures below room temperature, the coolant was used to lower the vapor temperature to the test condition, and then the heater was turned on. After the coolant temperature had stabilized, the heat input was slowly increased in increments of approximately 50 W until the heat input was close to the capillary limit. The heat input increments were then changed to 5–10 W until the capillary limit was reached. The heat pipe was allowed

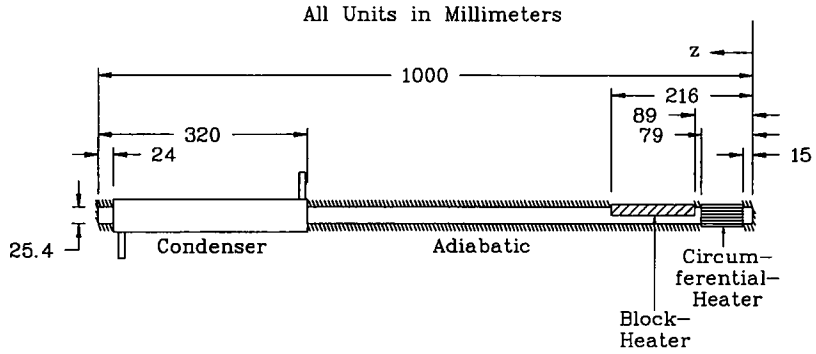

FIG. 2. Experimental heat pipe configuration.

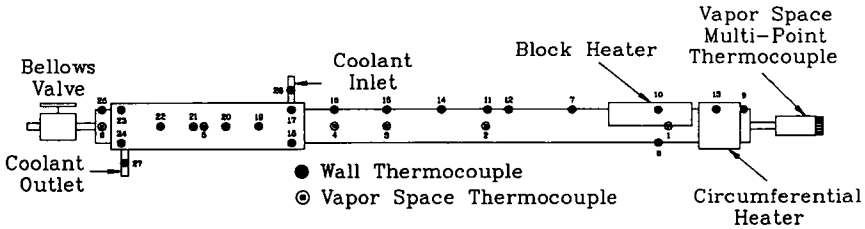

All distances measured from evaporator end cap

TC	Location (mm)	TC	Location (mm)	TC	Location (mm)
1	125	10	140	19	750
2	403	11	400	20	800
3	554	12	368	21	850
4	634	13	52	22	900
5	834	14	470	23	960
6	990	15	554	24	960
7	271	16	634	25	990
8	140	17	700	26	n/a
9	10	18	700	27	n/a

FIG. 3. Heat pipe thermocouple locations.

to reach steady-state conditions at each heat input by waiting a minimum of 20 min after the vapor temperatures had stabilized. The temperature directly underneath the heater was allowed to continuously rise for 25°C to verify that the wick had dried out. Two runs were performed for each vapor temperature under each heating mode to assure repeatability.

3. GENERALIZED ANALYTICAL PREDICTION OF CAPILLARY LIMIT FOR BLOCK HEATING

A simple, two-dimensional analysis was developed to predict the capillary limit based on the physical and material properties of the pipe, wick, and working fluid. The following assumptions were made: uniform heat addition in the heated region and heat removal in the condenser section, uniform vapor and liquid temperatures, laminar liquid and vapor flow, steady-state operation, and axisymmetric liquid flow about the centerline in the wick of the adiabatic and condenser sections. This analysis does not assume an axisymmetric liquid flow about the centerline in the evaporator section. This development is an extension of the conventional method by Chi [4] for circumferential heating to block heating. The pressure balance in a closed heat pipe is:

$$P_c(z) = [P_v(z) - P_v(z_{ref})] + [P_l(z_{ref}) - P_l(z)]. \quad (1)$$

As the heat load increases, the capillary pressure given by equation (1) increases. This is caused by the increase in the pressure difference between the liquid and vapor regions. For a given liquid–wick combination, the maximum capillary pressure generated is

$$P_{cm} = \frac{2\sigma}{r_p}. \quad (2)$$

The liquid pressure gradient is related to the frictional drag and the gravitational force [4]

$$[P_l(z) - P_l(z_{ref})] = \int_0^L (-F_l Q^* \pm \rho_l g \sin\psi)\, dz \quad (3)$$

where $z = 0$ refers to the condenser end cap and

$$F_l = \frac{\mu_l}{K A_w h_{fg} \rho_l}$$

$$K = \frac{d^2 \varepsilon^3}{122(1-\varepsilon)^2}$$

$$\varepsilon = 1 - \frac{\pi C D}{2(1+C)}$$

$$A_w = \frac{\pi}{4}(d_i^2 - d_w^2).$$

Similarly, the vapor pressure drop can be expressed in terms of the local axial heat flow rate.

$$[P_v(z_{ref}) - P_v(z)] = \int_0^L \left(F_v Q^* - D_v \frac{d(Q^*)^2}{dz}\right) dz \quad (4)$$

where

$$F_v = \frac{(f_v Re_v)\mu_v}{2A_v r_{h,v}^2 \rho_v h_{fg}}.$$

For cylindrical heat pipes

$$(f_v Re_v) = 16$$

$$A_v = \frac{\pi}{4} d_w^2$$

$$r_{h,v} = \frac{d_w}{2}.$$

For closed heat pipe systems [4]

$$\int_0^L -D_v \frac{d(Q^*)^2}{dz}\, dz = 0$$

so equation (4) simplifies to

$$[P_v(z_{ref}) - P_v(z)] = \int_0^L F_v Q^*\, dz. \quad (5)$$

In the block-heated heat pipe, the circumferential distribution of the local axial heat rate is not uniform in the evaporator section, therefore, the local axial heat rate is defined as:

$$Q^*(z) = \int_0^{2\pi} Q'(z,\theta) R_{ave}\, d\theta \quad (6)$$

where $Q'(z,\theta)$ is the axial heat rate per unit circumferential length and R_{ave} is the average radius of the liquid–wick.

The maximum possible capillary pressure is reduced by the effects of the gravitational field on the circumferential movement of liquid in the wick [4].

$$P_{pm} = P_{cm} - P_n \quad (7)$$

where

$$P_n = \rho_l g d_i \cos\psi. \quad (8)$$

Substituting equations (2), (3), (5), (7), and (8) into equation (1) and assuming a zero inclination angle yields

$$\frac{2\sigma}{r_p} - \rho_l L g d_i = \int_0^L (F_v Q^* + F_l Q^*)\, dz.$$

Collecting the constants and substituting equation (6) gives

$$\frac{\dfrac{2\sigma}{r_p} - \rho_l L g d_i}{F_v + F_l} = \int_0^L Q^*\, dz = \int_0^L \int_0^{2\pi} Q'(z,\theta) R_{ave}\, d\theta\, dz. \quad (9)$$

The capillary limit is determined by integrating equa-

tion (9) and then solving the resulting equation for the capillary limit. In the uniform, circumferentially-heated heat pipe, the integral with respect to $d\theta$ simplifies to a constant times $Q^*(z)$ since $Q'(z,\theta)$ is uniform in the circumferential direction.

$$Q^*(z) = Q'(z,\theta)2\pi R_{ave}. \tag{10}$$

For the circumferentially-heated heat pipe equation (9) becomes

$$\frac{\frac{2\sigma}{r_p} - \rho_l L g d_i}{F_v + F_l} = \int_0^L Q^*(z)\,dz. \tag{11}$$

For the block-heated heat pipe, the capillary heat transport factor is two-dimensional in the evaporator, so $Q'(z,\theta)$ is defined for each section of the heat pipe. For the condenser and adiabatic sections, a uniform axial heat rate is assumed.

For $0 \leqslant z \leqslant L_c$

$$Q'(z,\theta) = \frac{Q_{c,max}}{2\pi R_{ave}} \frac{z}{L_c}. \tag{12}$$

For $L_c \leqslant z \leqslant L_c + L_a$

$$Q'(z,\theta) = \frac{Q_{c,max}}{2\pi R_{ave}}. \tag{13}$$

Two separate equations are needed for the axial heat rate per unit circumferential distance for the heated region and the insulated region in the evaporator section. The uniform radial heat flux in the heated region creates a linear relationship in the axial heat rate from the uniform value at the adiabatic/evaporator section boundary to zero at the evaporator end cap. The heat rate per unit circumferential length in the heated region of the evaporator section is described by the following equation.

For $L_c + L_a \leqslant z \leqslant L$ and $0 \leqslant \theta \leqslant \pi$

$$Q'(z,\theta) = \left(\frac{L-z}{L_c}\right)\left(\frac{1}{\pi R_{ave}}\right)\left(\frac{Q_{c,max}}{2}\right). \tag{14}$$

Since there is no heat transfer through the walls of the insulated region of the evaporator section, the liquid must be transported from the insulated region to the heated region before it can be evaporated. An average transport length was developed from the maximum and minimum transport lengths. The minimum transport length is along the interface between the heated and insulated regions of the liquid–wick and is equal to the evaporator length. The maximum transport length in the evaporator occurs for flow entering the evaporator section directly opposite of the center of the heater. The maximum travel length for this flow is the evaporator length plus one half the circumference. The average of these two values is

$$\frac{(L)+(L+\pi R_{ave})}{2} = L + \frac{\pi}{2} R_{ave}. \tag{15}$$

Equation (15) was then used to determine a linear equation for $Q'(z,\theta)$ in the insulated region of the evaporator.

For $L_c + L_a \leqslant z \leqslant L_{eff}$ and $\pi \leqslant \theta \leqslant 2\pi$

$$Q'(z,\theta) = \left(\frac{L_{eff}-z}{L_c + \frac{\pi}{2}R_{ave}}\right)\left(\frac{1}{\pi R_{ave}}\right)\left(\frac{Q_{c,max}}{2}\right) \tag{16}$$

where L_{eff} is the effective travel length and is equal to $L+(\pi/2)R_{ave}$ in this case. $Q'(z,\theta)$ is then substituted into equation (9) and a solution is found in terms of $Q_{c,max}$.

$$\begin{aligned}\frac{\frac{2\sigma}{r_p} - \rho_l L g d_i}{F_v + F_l} &= \int_0^{2\pi}\int_0^{L_c}\left(\frac{Q_{c,max}}{2\pi L}\right)\left(\frac{z}{L_c}\right)dz R_{ave}\,d\theta \\ &+ \int_0^{2\pi}\int_{L_c}^{L_c+L_a}\left(\frac{Q_{c,max}}{2\pi R_{ave}}\right)dz R_{ave}\,d\theta \\ &+ \int_0^{\pi}\int_{L-L_c}^{L}\left(\frac{L-z}{L_c}\right)\left(\frac{1}{\pi R_{ave}}\right)\left(\frac{Q_{c,max}}{2}\right)dz R_{ave}\,d\theta \\ &+ \int_{\pi}^{2\pi}\int_{L-L_c}^{L_{eff}}\left(\frac{L+\frac{\pi}{2}R_{ave}-z}{L_c+\frac{\pi}{2}R_{ave}}\right)\left(\frac{1}{\pi R_{ave}}\right) \\ &\times\left(\frac{Q_{c,max}}{2}\right)dz R_{ave}\,d\theta\end{aligned}$$

$$Q_{c,max} = \frac{\frac{2\sigma}{r_p} - \rho_l L g d_i}{\left(\frac{L_c}{2} + L_a + \frac{L_c}{2} + \frac{\pi}{8}R_{ave}\right)}. \tag{17}$$

The term $(\pi/8)R_{ave}$ in the denominator of equation

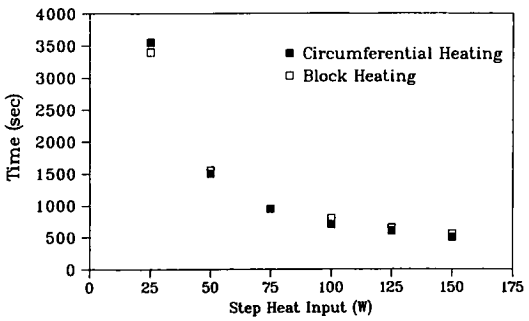

FIG. 4. Time for heat pipe vapor temperature to reach 60°C vs step heat input.

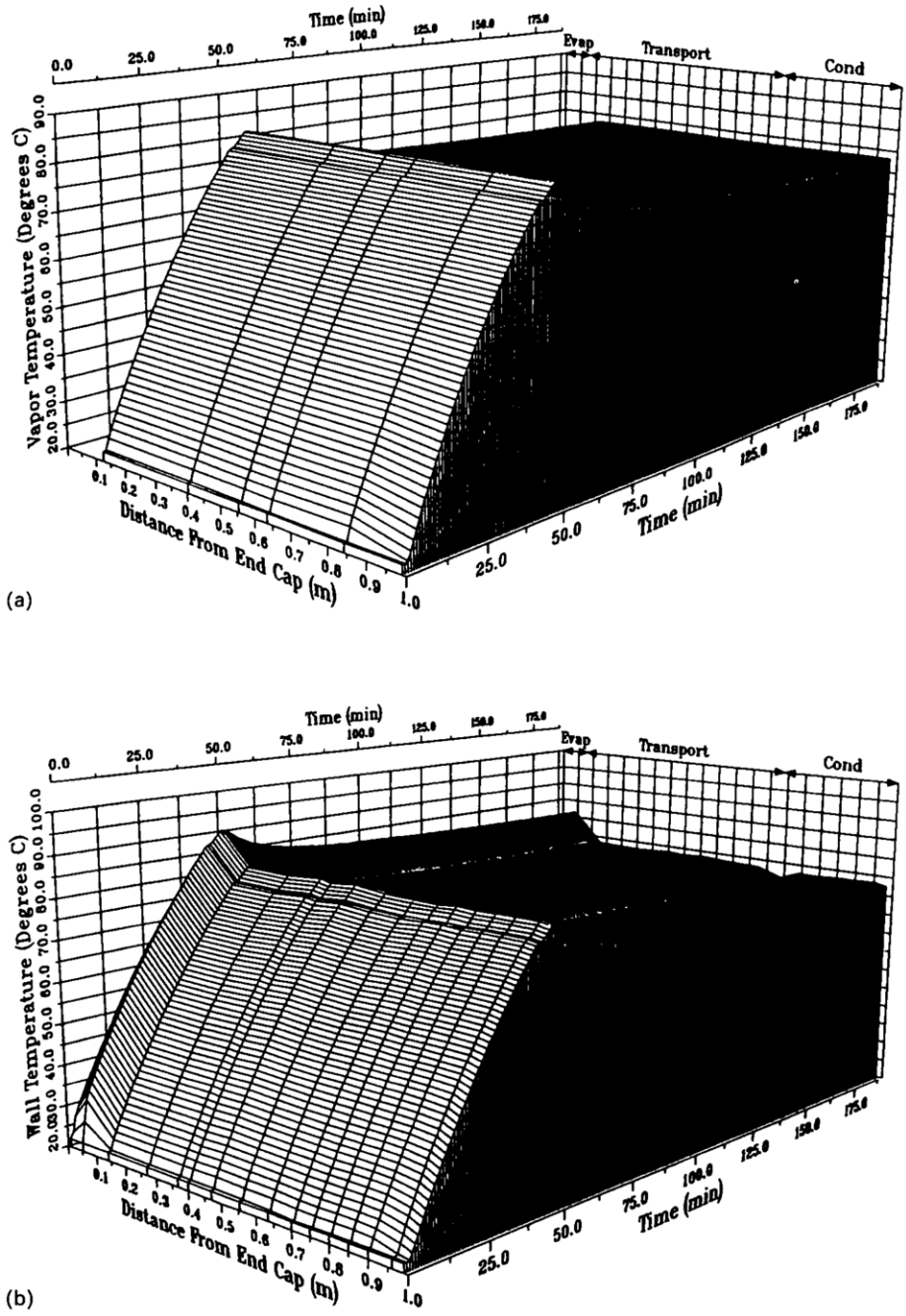

FIG. 5. Transient starting temperature profiles of the circumferentially-heated heat pipe for 50 W. (a) Vapor temperatures. (b) Wall temperatures.

(17) cancels out during the integration for circumferential heating and the resulting equation is identical to that given by Chi [4].

4. RESULTS AND DISCUSSION

The time needed for the heat pipe vapor temperature to reach 60°C was recorded under circumferential heating and block heating. These records led to the following: a comparison of the elapsed time between the two modes of heating is discussed; the vapor and wall temperatures during the transient start-up and the steady-state conditions are presented; the experimental and analytical capillary limits using both modes of heating were determined for several vapor temperatures; a comparison between the two modes of heating and between the analytical and experimental results is made.

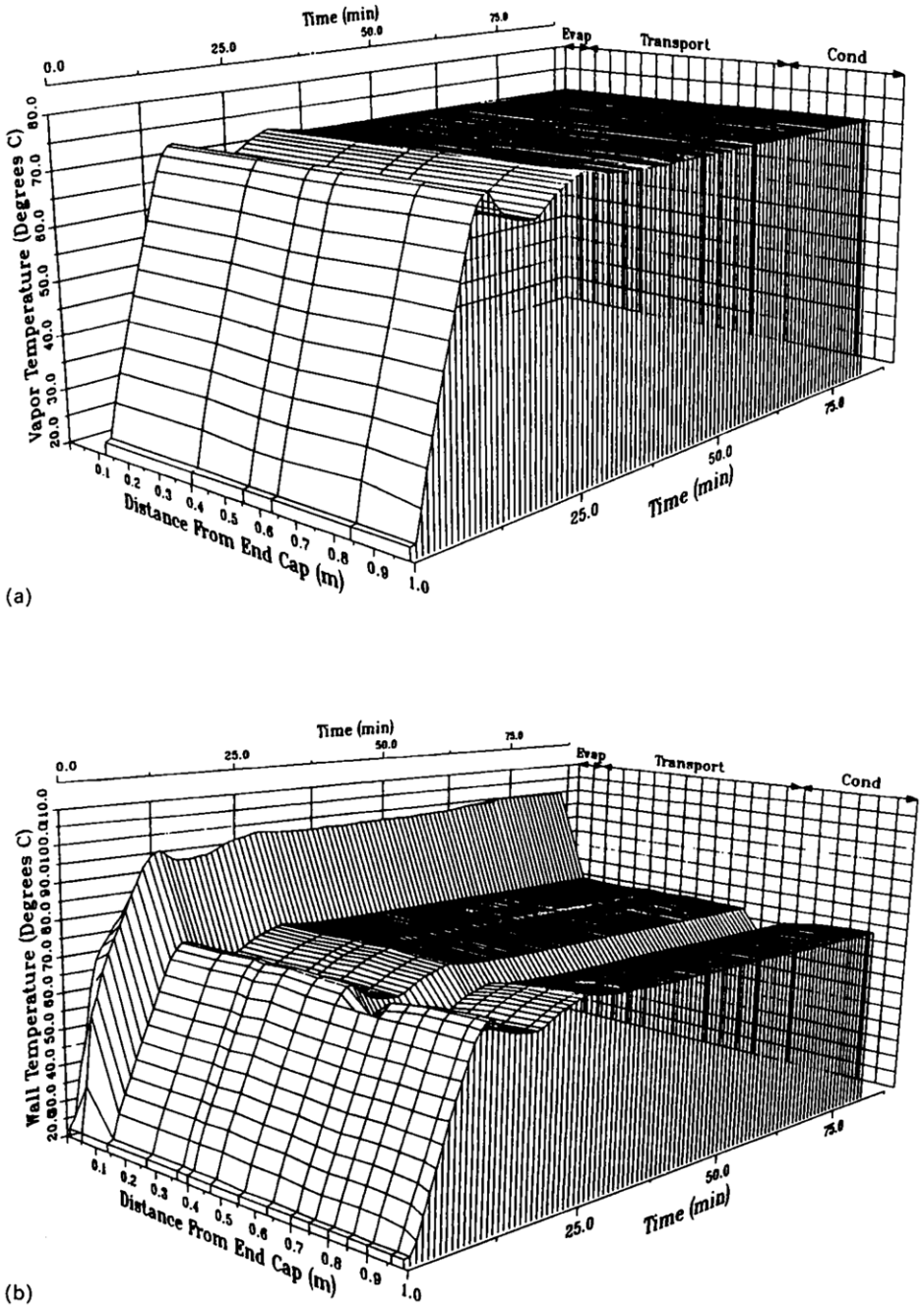

FIG. 6. Transient starting temperature profiles of the circumferentially-heated heat pipe for 150 W. (a) Vapor temperatures. (b) Wall temperatures.

4.1. *Elapsed time to* 60°C *vapor temperature*

Figure 4 presents the time required for the heat pipe vapor temperature to reach 60°C to compare the transient response of the heat pipe in circumferential and block heating modes. There was no significant difference in the response time between the two operating modes. The differences that were seen can be attributed to the variations in the starting vapor temperature and the resolution of the transient data. The data were taken at 50 s intervals and so the resolution of the transient data was limited to ± 50 s. This was the minimum time required by the data recording instrumentation for the calculation, display, and recording of the temperatures. The starting temperature of the heat pipe varied from 21 to 24°C. By an energy balance it can be seen that as heat was put into the heat pipe and no heat removed by the condenser, the internal energy of the heat pipe increased. As the heat

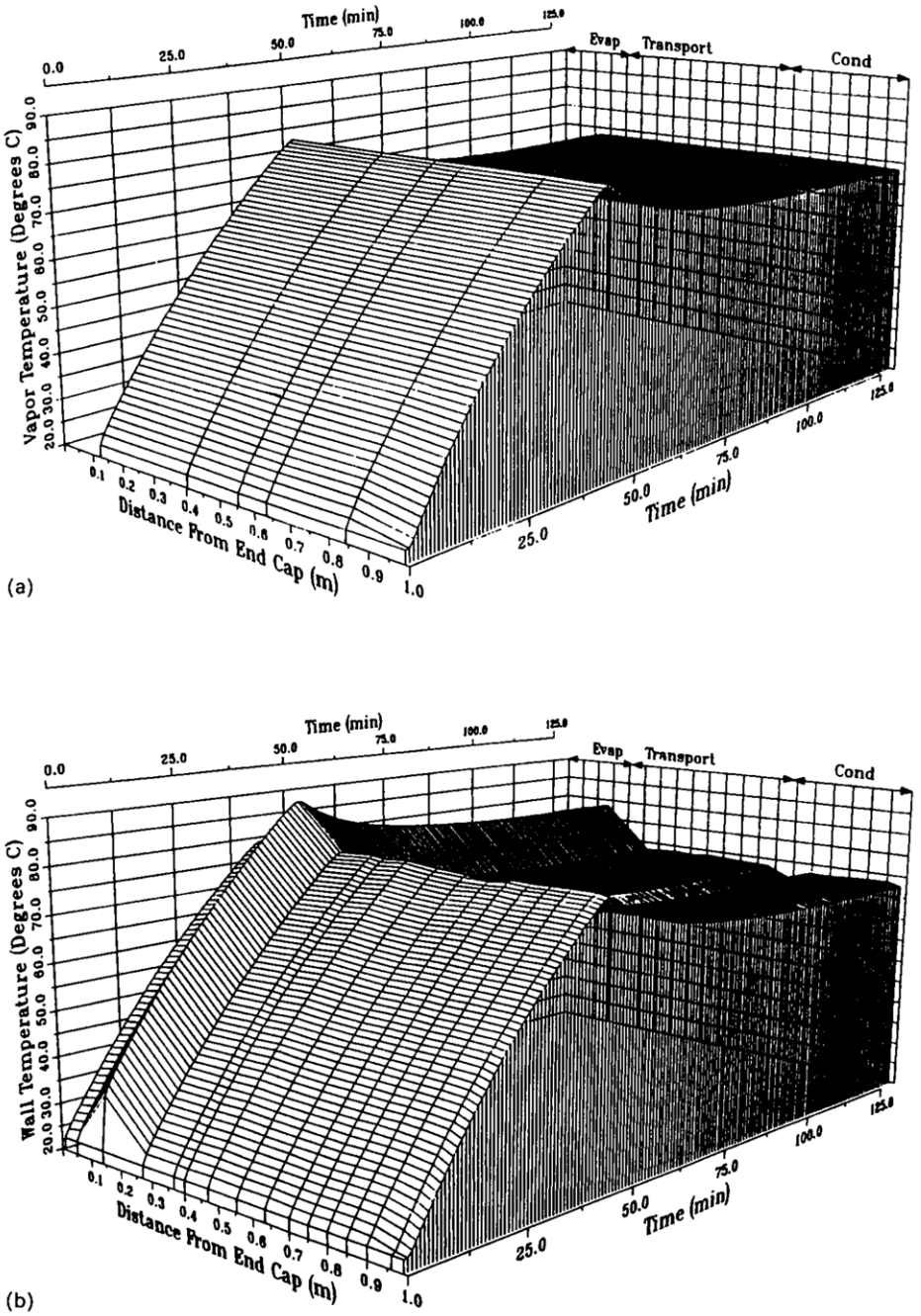

FIG. 7. Transient starting temperature profiles of the block-heated heat pipe for 50 W. (a) Vapor temperatures. (b) Wall temperatures.

input was increased, the rate at which the internal energy rose also increased and therefore the vapor temperature rose more quickly. It was concluded that the heat pipe time response to a step heat input was the same for both heating modes.

4.2. *Transient and steady-state temperature comparisons*

The transient vapor and wall temperatures for step heat inputs of 50 and 150 W are shown in Figs. 5 and 6 for circumferential heating, and in Figs. 7 and 8 for block heating, respectively. The wall temperatures shown in these figures are from the top of the heat pipe. The transient vapor centerline temperature profiles for both circumferential (Figs. 5(a) and 6(a)) and block heating (Figs. 7(a) and 8(a)) modes show very little axial variance in the vapor temperature of the heat pipe at these heat inputs. This flat axial profile is common in low temperature heat pipes in which no noncondensable gases are present in the heat pipe [2, 4].

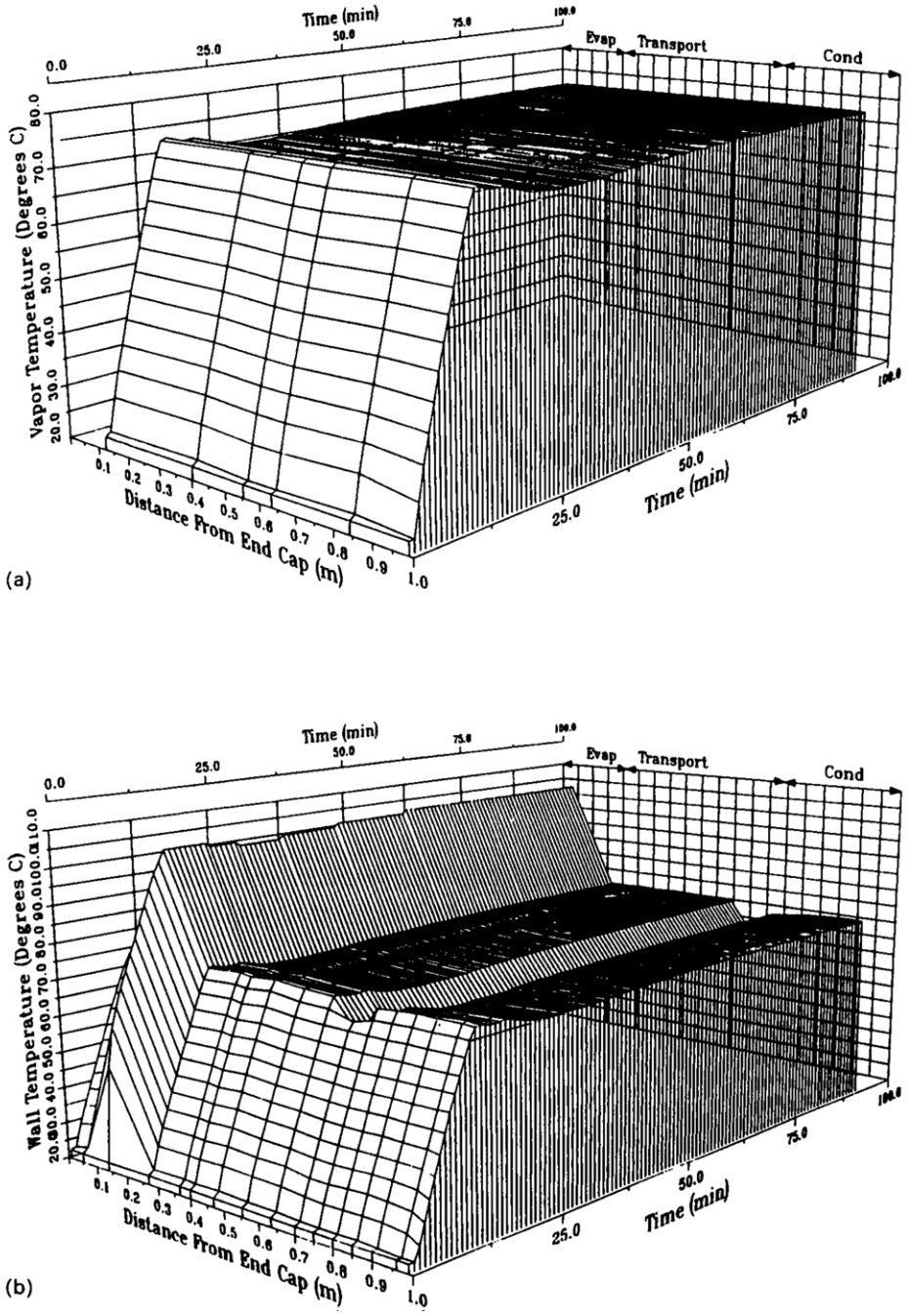

FIG. 8. Transient starting temperature profiles of the block-heated heat pipe for 150 W. (a) Vapor temperatures. (b) Wall temperatures.

The transient wall temperature profiles for both circumferential (Figs. 5(b) and 6(b)) and block heating (Figs. 7(b) and 8(b)) modes show that the temperature spike directly underneath the heater develops almost immediately upon the application of heat. Also, the remainder of the wall temperatures remain axially uniform throughout the transient period. Except for the fact that the peak temperature in the block heating mode was higher than the circumferential heating mode for a given heat input, there were no significant differences observed in the transient response of the heat pipe.

After the coolant had been started through the condenser, the heat pipe was allowed to reach a steady-state condition. Figures 9 and 10 show a comparison of the initial and final wall and vapor temperatures for both heating modes for heat inputs of 50 and 150 W. No effort was made to match the final vapor

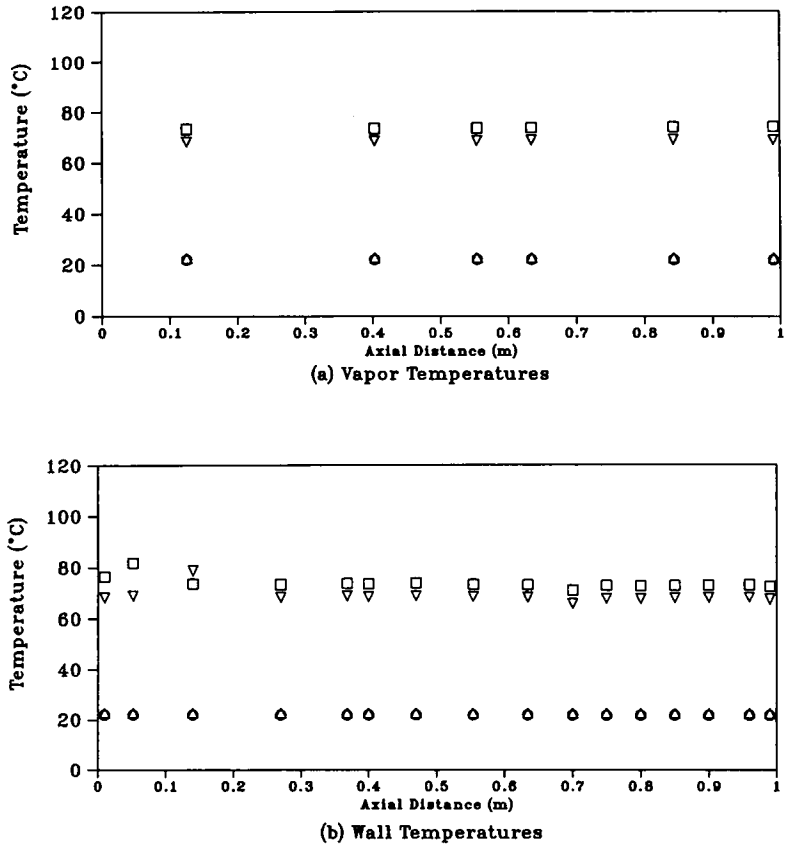

FIG. 9. Vapor and wall temperature vs axial distance from evaporator end cap for 50 W step heat input.

temperatures between the circumferential and block heating modes. Instead, a constant coolant flow rate and constant inlet temperature were maintained for each heat input. This was the cause for the slight difference in the steady-state vapor and wall temperatures in the 50 W heat input test. When this difference was taken into account, it was determined that the steady-state vapor and wall temperatures for both heating modes were similar, except for the wall temperatures in the region around the evaporator. Since the two evaporators were not in the same physical location, the difference in the location of the wall temperature peaks was expected. The peak wall temperature for the block-heated mode was higher than the circumferentially-heated mode for all heat inputs studied.

At the higher heat inputs, a temperature trough developed at the beginning of the condenser section when the coolant was allowed to flow through the condenser. This was caused by the large temperature difference between the coolant inlet temperature and the wall temperature at the beginning of the condenser.

4.3. *Capillary limit*

The experimentally determined capillary limits for both modes of heating were compared with the analytical predictions with good agreement. The physical dimensions of the heat pipe and the material properties of water were substituted into equation (17) and the analytical capillary limit was determined for several vapor temperatures as shown in Fig. 11. The experimental capillary limits are also shown in this figure.

The analytical methods used to determine the capillary limits were in agreement with the experimental data for both heating modes. For the block-heated experiment, the experimental capillary limit at 20°C vapor temperature was unobtainable because of insufficient coolant flow capacity in the condenser. The experimental capillary limits for the block heating mode at 80 and 100°C could not be determined

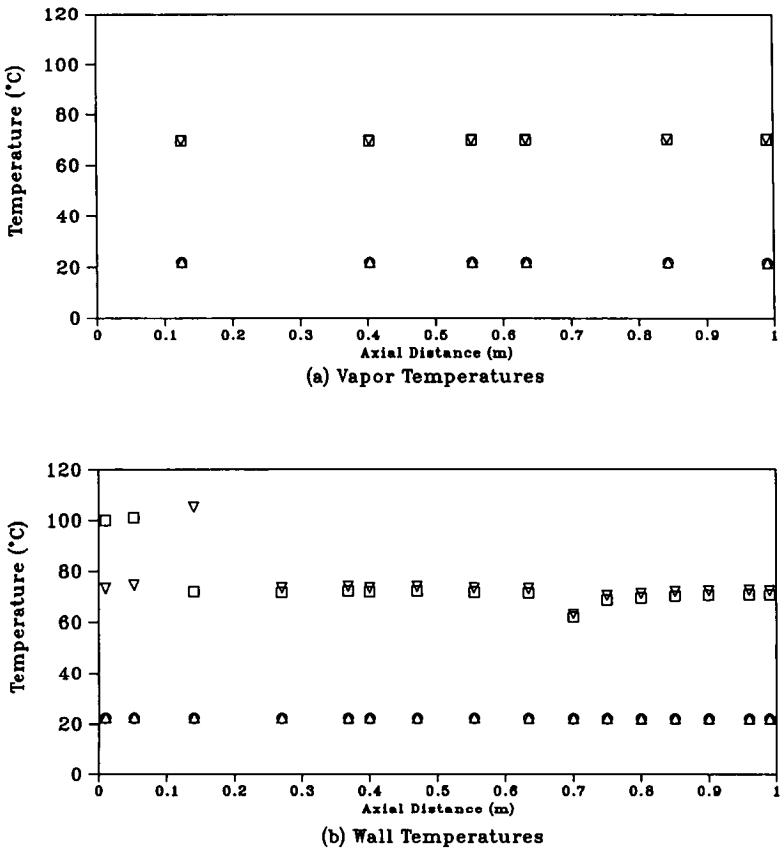

FIG. 10. Vapor and wall temperature vs axial distance from evaporator end cap for 150 W step heat input.

because the limit was above the maximum heat input of the heater. For the experimental capillary limits reported, there was good agreement with the analytical calculations. The analytical prediction provides a conservative estimation of the capillary limit of the heat pipe under block heating. There was a maximum error of 10% between the experimental limits and the analytical limits for the circumferentially-heated heat pipe, and a maximum of 25% for the block-heated heat pipe.

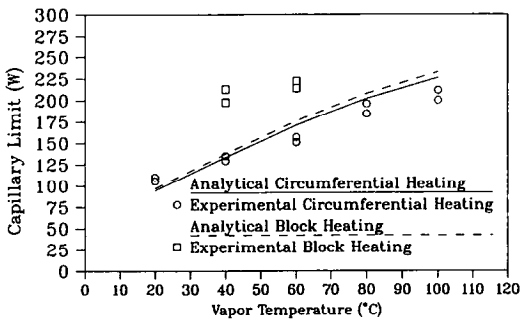

FIG. 11. Analytical and experimental capillary limit vs vapor temperature for circumferential and block heating modes.

The experimental capillary limits for block heating are higher than those for circumferential heating. This was partially caused by the shorter adiabatic section in the block-heated heat pipe. Faghri and Buchko [2] showed that decreasing the adiabatic transport length significantly increased the capillary limit. The analytical capillary limits calculated for this study also show this trend. It was observed in both the analytical and experimental predictions that there was a significant increase in the capillary limit for both modes of heating as the vapor temperature increased. This was due to the decrease of the viscosity of liquid water.

5. CONCLUSIONS

A copper–water heat pipe with both circumferential and block heaters was used to determine several transient and steady operating characteristics under each

heating mode. There were only very small differences in the elapsed time for the heat pipe to reach 60°C between the circumferential heating and block heating modes, with the largest differences seen at the low heat inputs. The vapor temperatures remained within 1°C of each other during the entire transient start-up. The fast time response of the heat pipe to block heating makes it as effective in electronic cooling as other conventional applications. The peak wall temperature during transient start-up for the block-heated heat pipe was slightly higher than the circumferentially-heated heat pipe. The vapor and wall temperatures at steady state were not significantly different either, except for the wall temperatures in the region around the evaporator.

The experimental capillary limits determined for a copper–water heat pipe in circumferential and block heating modes were compared with the analytical values calculated using equation (17). The analytical predictions were within 25% of the experimental limits. The capillary limits for block-heated operation were slightly higher than the circumferentially-heated limits. This can be partially attributed to the shorter adiabatic transport section of the block-heated heat pipe. The capillary limit increased significantly with an increase in vapor temperature for both heating modes.

Acknowledgement—Funding for this research was provided by a joint effort of the NASA Lewis Research Center and Thermal Energy Group of the Aero Propulsion Laboratory of the U.S. Air Force under contract F33615-89-C-2820.

REFERENCES

1. A. Faghri and S. Thomas, Performance characteristics of a concentric annular heat pipe, part II, vapor flow analysis, *ASME J. Heat Transfer* **11**, 851–857 (1989).
2. A. Faghri and M. Buchko, Experimental and numerical analysis of low temperature heat pipes with multiple heat sources, *ASME J. Heat Transfer* **113**, 728–734 (1991).
3. J. H. Rosenfeld, Modeling of heat transfer into a heat pipe for a localized heat input zone, *Proc. A.I.Ch.E. Symp. Series, Heat Transfer* **83**, 71–76 (1987).
4. S. W. Chi, *Heat Pipe Theory and Practice; A Sourcebook*, McGraw-Hill, New York (1976).